Earth and Planetary Science Letters 404 (2014) 396–407

Contents lists available at ScienceDirect

Earth and Planetary Science Letters

www.elsevier.com/locate/epsl

Iron isotope tracing of mantle heterogeneity within the source regions of oceanic basalts

Helen M. Williams [a,*], Michael Bizimis [b]

[a] Department of Earth Sciences, Durham University, Durham, DH1 3LE, UK
[b] Department of Earth and Ocean Sciences, University of South Carolina, Columbia, SC 29208, USA

ARTICLE INFO

Article history:
Received 19 June 2013
Received in revised form 23 July 2014
Accepted 29 July 2014
Editor: T. Elliott

Keywords:
Hawaii
pyroxenite
peridotite
iron isotope
primitive mantle

ABSTRACT

Mineralogical variations in the Earth's mantle and the relative proportions of peridotitic versus enriched and potentially crustally-derived pyroxenitic domains within the mantle have important implications for mantle dynamics, magma generation, and the recycling of surface material back into the mantle. Here we present iron (Fe) stable isotope data (δ^{57}Fe, deviation in ^{57}Fe/^{54}Fe from the IRMM-014 standard in parts per thousand) for peridotite and garnet–pyroxenite xenoliths from Oahu, Hawaii and explore Fe isotopes as tracer of both peridotitic and pyroxenitic components in the source regions of oceanic basalts. The pyroxenites have δ^{57}Fe values that are heavy (0.10 to 0.27‰) relative to values for mid-ocean ridge and ocean island basalts (MORB; OIB; δ^{57}Fe ~ 0.16‰) and the primitive mantle (PM; δ^{57}Fe ~ 0.04‰). Pyroxenite δ^{57}Fe values are positively correlated with bulk pyroxenite titanium and heavy rare earth element (REE) abundances, which can be interpreted in terms of stable isotope fractionation during magmatic differentiation and pyroxene cumulate formation. In contrast, the peridotites have light δ^{57}Fe values (−0.34 to 0.14‰) that correlate negatively with degree of melt depletion and radiogenic hafnium isotopes, with the most depleted samples possessing the most radiogenic Hf isotope compositions and lightest δ^{57}Fe values. While these correlations are broadly consistent with a scenario of Fe isotope fractionation during partial melting, where isotopically heavy Fe is extracted into the melt phase, leaving behind low-δ^{57}Fe peridotite residues, the extent of isotopic variation is far greater than predicted by partial melting models. One possibility is derivation of the samples from a heterogeneous source containing both light-δ^{57}Fe (relative to PM) and heavy-δ^{57}Fe components. While pyroxenite is a viable explanation for the heavy-δ^{57}Fe component, the origin of the depleted light-δ^{57}Fe component is more difficult to explain, as melting models predict that even large (>30%) degrees of melt extraction do not generate strongly fractionated residues. Multiple phases of melt extraction or other processes, such as metasomatism, melt percolation or the assimilation of xenocrystic olivine with light δ^{57}Fe values may need to be invoked to explain these light δ^{57}Fe values; a caveat to this is that these processes must either preserve, or generate correlations between δ^{57}Fe and Hf isotopes. Published variations in δ^{57}Fe in mantle melting products, such as MORB and OIB, are also greater than predicted by melting models assuming derivation from δ^{57}Fe-homogeneous mantle. For example, OIB from the Society and Cook-Austral islands, which have radiogenic Pb and Sr isotope compositions indicative of recycled components such as subduction modified, low-Pb oceanic crust and terrigenous sediments have heavy mean δ^{57}Fe values (~0.21‰) significantly distinct to those of other OIB and MORB, which could explained by the presence of heavy-δ^{57}Fe pyroxenite cumulate or pyroxenitic melt components, whereas large degree partial melts, such as komatiites and boninites, display light Fe-isotopic compositions which may reflect sampling of refractory, light-δ^{57}Fe mantle components. Iron stable isotopes may therefore provide a powerful new means of fingerprinting mineralogical variations within the Earth's mantle and identifying the mineralogy of depleted and enriched components within the source regions of volcanic rocks.

1. Introduction

Mineralogical variation in the Earth's upper mantle and the potential existence of enriched (pyroxenitic or eclogitic, pyroxene-dominated) and depleted (peridotitic, olivine-dominated) mantle

* Corresponding author. Tel.: +44 (0)191 334 2546; fax +44 (0)191 334 2546.
E-mail address: h.m.williams2@durham.ac.uk (H.M. Williams).

http://dx.doi.org/10.1016/j.epsl.2014.07.033

components has been the subject of debate for several decades (Allègre and Turcotte, 1986; Hauri, 1996; Hofmann and White, 1982; Workman et al., 2004). Numerous studies on erupted melts have used major and trace elements and short- or long-lived radiogenic nuclides to constrain mantle compositional and/or mineralogical variability (Elliott et al., 2007; Hauri, 1996; Humayun et al., 2004; Jackson and Dasgupta, 2008; Prytulak and Elliott, 2007; Sigmarsson et al., 1998; Sobolev et al., 2005; Stracke et al., 1999; Vlastelic et al., 1999). However, while pyroxenitic or eclogitic components are often invoked to account for the enriched isotopic signatures of oceanic basalts (Allègre and Turcotte, 1986; Hauri et al., 1996; Hirschmann and Stolper, 1996; Lassiter and Hauri, 1998; Lundstrom et al., 1999; Niu et al., 1999; Prinzhofer et al., 1989; Zindler et al., 1979; Zindler et al., 1984), their roles in generating mantle chemical heterogeneity remain controversial, as few independent tracers of source mineralogy exist, such that resolving compositional (trace element or radiogenic isotope) enrichment from mineralogical enrichment is challenging. For example, radiogenic isotope systems such as Sr, Nd, Hf and Pb can fingerprint crustally-derived components, but cannot distinguish whether these components remain present as distinct lithological units (e.g. as pyroxenite or eclogite), or whether they are completely homogenized into the mantle by means of convective stirring (Gurenko et al., 2009; Jackson and Dasgupta, 2008) such that only their geochemical signals remain.

Pyroxenite source components can be generated from both crustal and mantle-sourced protoliths. 'Crustal' pyroxenite components may be directly derived from recycled oceanic crust as eclogite (Pertermann and Hirschmann, 2003) or may form by i) partial melting of subducted eclogite and the reaction of these melts with mantle peridotite to form garnet pyroxenite (Hauri, 1996; Huang and Frey, 2005; Sobolev et al., 2005); this scenario has been invoked to explain the high SiO_2 and Ni contents and high Fe/Mn ratios of some Hawaiian basalts (Sobolev et al., 2007; Sobolev et al., 2005), or ii) the extraction of silica-rich fluids or melts from oceanic crust during subduction (Kogiso et al., 2003). In contrast, 'mantle' pyroxenite components are considered to form as high-pressure cumulates of low-degree mantle melts that infiltrate and crystallize near the base of the oceanic mantle lithosphere (Niu and O'Hara, 2003; Pilet et al., 2008) or through interaction and melt–rock reaction between magmas and surrounding peridotite wall-rock (Downes, 2007). For clarity, we use the term "pyroxenite" to refer to source mineralogy (olivine-free, pyroxene and garnet-bearing) rather than source origin unless this is referred to specifically.

Depleted peridotitic components have also been invoked within the source regions of OIB and MORB. Several studies have suggested that the Hawaiian plume mantle source contains long-term depleted and compositionally variable peridotitic components (Bizimis et al., 2013, 2005; Pietruszka and Garcia, 1999; Ren et al., 2006; Stracke et al., 1999) and depleted components have also been invoked in the source of Reunion OIB (Vlastelic et al., 2006) and MORB. Evidence for the latter is provided by correlated Hf–Nd isotopes in MORB (Salters et al., 2011) and the radiogenic Hf isotope compositions of Gakkel Ridge abyssal peridotites (Stracke et al., 2011), while mantle peridotites found at mid-oceanic spreading centers and as xenoliths in OIB provide some of the strongest evidence for the presence of ancient depleted peridotites in the convecting mantle (Bizimis et al., 2007; Burton et al., 2012; Liu et al., 2008; Stracke et al., 2011). However, identifying the presence of depleted components in mantle source regions is not without difficulty. A major challenge is the low incompatible element concentrations of refractory mantle peridotites, which means that they have little influence on the incompatible trace element and radiogenic isotope budget of erupted melts (Burton et al., 2012). Another challenge relates to the ease with which the incompatible trace element and radiogenic isotope signature of mantle rocks can be overprinted by metasomatic processes with little or no change in mineralogy (Niu and O'Hara, 2003).

New tracers of both depleted and enriched mantle mineralogical components are thus required to compliment the extensive and rapidly growing evidence for mantle heterogeneity based on trace elements and radiogenic isotopes. Given the major advances that have been made in "heavy" (high atomic weight) metal stable isotope analyses over the last ten years, it is now timely to explore the use of these stable isotope systems as tracers of mantle heterogeneity. In this study, we explore the use of Fe stable isotopes as a tracer of mantle source mineralogy using peridotite and pyroxenite xenoliths from Hawaii as a case study.

1.1. Iron isotopes as a tracer of mantle mineralogical variations

Iron is a major cation in the Earth's mantle, with a bulk partition coefficient close to 1 (Herzberg, 2004; Keshav et al., 2004; Kogiso and Hirschmann, 2006; Pearce and Parkinson, 1993; Pertermann and Hirschmann, 2003; Sobolev et al., 2005; Weyer and Ionov, 2007). Consequently, Fe concentrations vary little with degree of melting (at constant pressure) in primary MORB melts (Klein and Langmuir, 1987) and peridotites (Ionov and Hofmann, 2007), at least for degrees of melting appropriate for present day MORB and OIB (generally $<$15–20%). Theoretical (Polyakov and Mineev, 2000) and empirical observations from equilibrated peridotites and pyroxenites (Weyer and Ionov, 2007; Williams et al., 2005) indicate that isotopically heavy Fe (high δ^{57}Fe; parts per thousand deviation in ^{57}Fe/^{54}Fe from the IRMM-14 iron standard) will be concentrated in both low- and high-Ca pyroxenes relative to olivine (by ca. 0.15 to 0.20‰; Weyer and Ionov, 2007; Williams et al., 2005) due to differences in bonding environment. As melting preferentially consumes pyroxene over olivine, peridotitic residues, melts and cumulates derived from melts of peridotitic and pyroxenitic source regions should inherit distinct Fe isotope signatures reflecting both the degree of melt extraction and the nature of the source mineralogy. Furthermore, as the Fe contents of melts derived from peridotitic and pyroxenitic mineralogies (e.g., Sobolev et al., 2005 their Table 1) are approximately similar, neither lithology should disproportionately contribute to the Fe budget of erupted melts and the Fe isotope compositions of primitive lavas should therefore primarily reflect the mineralogies of their respective source regions.

While mineral-specific Fe-isotope partitioning effects have been recognized in a number of earlier studies (Beard and Johnson, 2004; Teng et al., 2008; Weyer et al., 2005; Weyer and Ionov, 2007; Williams et al., 2004, 2009, 2005) the effects of variable source mineralogy have not yet been extensively explored in either models attempting to simulate Fe isotope fractionation during partial melting or in calculations of the Fe isotope composition of the Earth's mantle. Existing estimates of the Fe isotope composition of the Earth's mantle or the bulk silicate Earth (BSE) are constrained by sampling to the upper mantle and are generally based on suites of comparatively primitive basalts or their melting residues. In an early study (Weyer et al., 2005), it was observed that unmetasomatized peridotites from a variety of tectonic settings displayed near-chondritic δ^{57}Fe values whereas oceanic basalts displayed heavier δ^{57}Fe values (mean ~0.16‰), similar to those of high-Mg lunar basalts but heavier than the chondritic δ^{57}Fe values displayed by SNC meteorites and eucrites (Poitrasson et al., 2004; Schoenberg and von Blanckenburg, 2006; Weyer et al., 2005). Weyer et al. (2005) concluded that the mean peridotite δ^{57}Fe provided the best estimate of the BSE, noting that relative differences in planetary mantle δ^{57}Fe could only be estimated through comparisons of erupted basalts and their meteoritic

equivalents, as meteorites representing the residues of mantle partial melting on the Moon, Mars and Vesta are not available. In a latter study (Dauphas et al., 2009) the δ^{57}Fe value of the BSE was estimated i) by intersecting a correlation between δ^{57}Fe and Fe/Si in chondrites with the current Fe/Si estimated for the BSE, giving a BSE δ^{57}Fe value of 0.02 ± 0.07‰, and ii) from the mean δ^{57}Fe of boninites (0.04 ± 0.01‰), which as high-degree melts should approximate the isotopic composition of their source region. More recent estimates of the BSE have been obtained from abyssal peridotites (0.04 ± 0.04‰; Craddock et al., 2013) and the ~90 Ma Gorgona komatiite suite (-0.13 ± 0.05‰; Hibbert et al., 2012).

While all these estimates of the BSE δ^{57}Fe value are useful, they do not provide much information on the relative Fe isotope compositions of planetary mantles, as samples of comparable petrology have not yet been obtained from the other terrestrial planets and insufficient information is available regarding the degree to which Fe isotopes fractionate during mantle melting and the extent to which this may depend on variations in planetary mantle oxidation state and mineralogy. More critically, current estimates of BSE δ^{57}Fe do not constrain the potential variability in δ^{57}Fe that may exist in the Earth's mantle, let alone that of the other terrestrial planets. For example, do the mantle source δ^{57}Fe values estimated from either boninites (Dauphas et al., 2009) or the Gorgona komatiites (Hibbert et al., 2012) provide a true measure of PM or BSE δ^{57}Fe, or do they represent preferential sampling of more depleted, low-δ^{57}Fe domains within the mantle?

1.2. Models of Fe isotope fractionation during partial melting

Although there are, to our knowledge, no experimental studies of Fe isotope fractionation between silicate melts and minerals, it is widely observed that the products of partial melting (e.g. MORB and OIB) are displaced to higher δ^{57}Fe values (typically by 0.1–0.2‰) than unmetasomatized mantle peridotites (Dauphas et al., 2009; Weyer and Ionov, 2007; Williams et al., 2004, 2005). This effect could relate to the more incompatible nature of Fe^{3+} during melting (Dauphas et al., 2009; Williams et al., 2004), and/or to the non-modal nature of partial melting, where (isotopically heavier) pyroxene contributes disproportionately to the melting assemblage. The effects of non-modal melting can be explored with partial melting models where observed differences in δ^{57}Fe between equilibrated olivine and clinopyroxene in mantle peridotites and clinopyroxene and olivine in mantle eclogites (Weyer and Ionov, 2007; Williams et al., 2009, 2005) are used to approximate relative differences in mineral-melt Fe isotope partitioning. These differences reflect subsolidus mineral equilibration at temperatures ranging from ca. 900 to 1200 °C (Weyer and Ionov, 2007; Williams et al., 2009, 2005) rather than mantle potential temperatures and it may be expected that they will decrease with increasing temperature (as $1/T^2$). In the models discussed below, we have not applied a temperature correction due to the absence of experimental data describing the temperature dependence of inter-mineral Fe isotope fractionation and because no correlations between mineral fractionation factors and apparent equilibration temperature have been observed in the existing studies.

We use an incremental batch non-modal melting model (see Appendix A for details) where the modal mineralogy of the residue is recalculated at each melting increment. At each melting step the Fe-isotope fractionation between melt and residue is dictated by the melt and residue fractionation factor, α:

$$R_{\text{melt}} = \alpha_{\text{melt-residue}} * R_{\text{residue}} \quad (1)$$

Where R_{melt} and R_{residue} are the absolute $^{57}Fe/^{54}Fe$ isotopic compositions of the melt and the residue at any given melting increment. As melt-mineral α (and hence melt-residue) values are unknown, we recast $\alpha_{\text{melt-residue}}$ as a function of the fractionation factor between melt and clinopyroxene ($\alpha_{\text{melt-cpx}}$; $R_{\text{melt}}/R_{\text{cpx}}$), which we treat as a free variable, and subsolidus clinopyroxene-mineral fractionation factors ($\alpha_{\text{mineral-cpx}}$; $R_{\text{min}}/R_{\text{cpx}}$), which we estimate from observed differences in δ^{57}Fe between equilibrated phases in mantle peridotites, pyroxenites and eclogite xenoliths (Weyer and Ionov, 2007; Williams et al., 2009, 2005).

At each melting increment, the modal abundance of each phase (n, Eq. (2)) and its Fe concentration is calculated by mass balance from the original source mineralogy and mineral Fe contents coupled with literature partition coefficients for Fe. Melting reactions are defined using liquid modes (p values) where positive values indicate consumption during melting, negative values crystallization:

$$n_{\text{mineral residue}} = n_{\text{mineral initial}} - (F \times p_{\text{mineral}}) \quad (2)$$

where F = the degree of partial melting, and p describes the relative proportion of a given mineral in the melting reaction. Melting reactions for the lherzolite lithologies were taken from Robinson et al. (1998). Clinopyroxene is exhausted at 25% melting after which harzburgite melting modes (given in the Appendix A and based on the study of Parman and Grove, 2004) are used to take into account this change in lithology. The Fe content of the bulk residue is then calculated as the weighted sum of the residual mineral modal abundances (normalized to 100%) and their Fe contents. The fractionation factor between the melt and bulk residue, $\alpha_{\text{melt-residue}}$ is calculated at each melting increment using the Fe content of the bulk residue and the value assigned to $\alpha_{\text{melt-cpx}}$, where n = normalized mineral modal abundance:

$$\alpha_{\text{melt-residue}} = \alpha_{\text{melt-cpx}} * \left(\sum_{i=1}^{n} [n_i \cdot \text{FeO}_{\text{mineral}}] \Big/ \sum_{i=1}^{n} [n_i \cdot \alpha_{\text{min-cpx}} \cdot \text{FeO}_{\text{mineral}}] \right) \quad (3)$$

The isotopic compositions of the instantaneous melt and residue at each step can then be calculated using $\alpha_{\text{melt-residue}}$ and Eq. (1). The value of R_{melt} calculated at the first melting increment uses the initial isotopic composition assumed for the source (0.36259 or 0.04‰ relative to IRMM-14). The value of R_{residue} at this and subsequent melting increments is calculated by mass balance between the original source and value of R_{melt} calculated for the extracted melt. The concentration and isotope composition of the aggregate melt for any given melt fraction is calculated by the sum of the weighted melt increments. The model assumes that each melt increment is completely extracted and each subsequent melting step uses the concentration, modal abundances and Fe-isotope composition of the previous residue. The model is checked so that mass balance is satisfied, i.e. the combined sum of the concentration and isotope composition of the residue and cumulate melt equates to that of the original source.

This model approach ensures that at each step each mineral remains in isotope equilibrium with the melt and the other minerals in the residue. Note that $\alpha_{\text{melt-residue}}$ is not simply a weighted average of $\alpha_{\text{melt-min}}$ values; rather it is dictated by the equilibrium with the mineral assemblage, and buffered by the presence of each mineral. Although this calculation does not implicitly model the greater incompatibility of Fe^{3+} during partial melting relative to Fe^{2+} (Woodland and Koch, 2003) or the preferential concentration of isotopically heavy Fe into Fe^{3+}-bonding environments (Polyakov et al., 2007; Polyakov and Mineev, 2000), these effects are allowed for via the dominance of clinopyroxene in the melting assemblage relative to olivine.

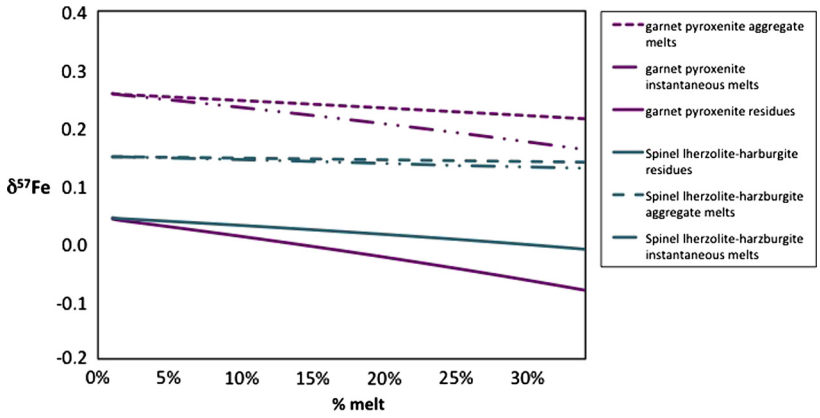

Fig. 1. Melt and residue δ^{57}Fe values generated by fractional melting of a primitive mantle source of δ^{57}Fe = 0.04‰ plotted against degree of partial melting, or mole fraction (F) of FeO removed for $\alpha_{\text{melt-cpx}} = 1$. Mineral modes, liquid modes, iron contents and isotopic compositions used in the models are given in Table A.1. Both lherzolite and pyroxenite sources were constrained to have initial δ^{57}Fe values of 0.04‰ in line with the current PM estimate and both sources also have the same starting FeO contents of 8.3 wt%.

The calculated δ^{57}Fe values of the evolving residues and associated melts are shown in Fig. 1, for fertile lherzolite and pyroxenite mineralogies with the same initial Fe isotope compositions and bulk FeO contents (detailed in the Appendix A). The results show that pyroxenite melts are heavier than lherzolitic partial melts at the same degree of partial melting (e.g. for $F = 0.10$ and $\alpha_{\text{melt-cpx}} = 1$, lherzolite and pyroxenite melts have δ^{57}Fe values of 0.15 and 0.25‰, respectively) although the difference decreases with increasing degree of melting. At a wide range of melting degrees ($0.01 < F < 0.25$) for $\alpha_{\text{melt-cpx}} = 1$, instantaneous and aggregate melts calculated for the lherzolite source show limited variation in δ^{57}Fe, with values ranging from 0.141 to 0.149 and 0.131 to 0.149‰. Melting residues also display a limited range in δ^{57}Fe, from 0.008 to 0.040‰. Increasing the value of $\alpha_{\text{melt-cpx}}$ increases the δ^{57}Fe values of the calculated melts and the difference in δ^{57}Fe between melt and residue, although it should be noted that $\alpha_{\text{melt-cpx}}$ values >1 are not required to explain the observed offset in δ^{57}Fe between mean MORB or OIB and mantle peridotites. The models therefore demonstrate that non-modal partial melting scenarios, where the melting phases is dominated by clinopyroxene, can readily explain the observed offset in δ^{57}Fe between mean MORB or OIB and mantle peridotites without requirement for additional mineral-melt fractionation. Critically, the models also predict that there will be minimal variation in the δ^{57}Fe values of erupted melts and residues across a wide range in melting degree.

Models of Fe isotope fractionation during partial melting have been presented in other studies (Weyer and Ionov, 2007; Williams et al., 2009, 2005), most recently by Dauphas et al. (2009). The latter study differs from our own in that it does not use data from natural samples and it does not take into account relative Fe isotope partitioning between minerals; rather Fe isotope fractionation is driven by differences in Fe^{3+}–Fe^{2+} partitioning, where it is assumed that the magnitude of fractionation between Fe^{3+}_{melt} and Fe^{3+}_{source} is ca 0.30‰ (for δ^{56}Fe, to convert to δ^{57}Fe the value would be 0.45‰) and there is no fractionation between Fe^{2+}_{melt} and Fe^{2+}_{source}. Both these models and our models can account for the observed difference in MORB and OIB from mantle peridotites. The slight difference between our models and those of Dauphas et al. (2009) may stem from the fact we have not incorporated an additional α term to allow for the more incompatible behavior of Fe^{3+}, although, as emphasized above, our models do take the behavior of Fe^{3+} into account indirectly, though the greater contribution of clinopyroxene to the melting assemblage.

1.3. The Fe isotope composition of the primitive mantle

As discussed above, MORB and OIB have heavy δ^{57}Fe (Beard et al., 2003; Dauphas et al., 2009; Teng et al., 2008, 2013; Weyer et al., 2005) relative to mantle peridotites (Craddock et al., 2013; Weyer et al., 2005; Williams et al., 2005) and chondrites (Dauphas et al., 2009). While this difference is qualitatively consistent with melting models, the overall range in δ^{57}Fe displayed by MORB and OIB (Fig. 2) is over 0.2‰ and 0.4‰, respectively, for a restricted range of MgO contents (see Figure caption for details), and is substantially greater than that predicted in our melting models and those of Dauphas et al. (2009) and is much larger than can be explained by analytical uncertainty or processes such as fractional crystallization (Schuessler et al., 2009), olivine accumulation (Teng et al., 2008) and fluid exsolution (Heimann et al., 2008). A similar discrepancy also exists for melting residues as the δ^{57}Fe variation displayed by fresh abyssal peridotites (Craddock et al., 2013), commonly thought to represent the residues of MORB-melt extraction, is 0.24‰, far greater than that predicted by any model.

One explanation for this observed variability in melt and residue δ^{57}Fe is derivation of these samples from a δ^{57}Fe-heterogeneous mantle, as previously suggested for Ko'olau OIB (Teng et al., 2013). In order to evaluate the potential for mantle Fe-isotope heterogeneity, the underlying causes of that heterogeneity and the suitability of Fe isotopes as a tracer of mantle mineralogy the following questions need to be addressed: i) the extent of Fe-isotope variation that exists between different mantle lithologies; ii) the nature of the processes generating Fe isotope variations between and within different mantle lithologies and iii) the extent to which mantle region source Fe-isotope heterogeneity can explain the variations in δ^{57}Fe observed in oceanic basalts.

To address these questions we have determined the Fe isotope compositions of silicate minerals (Table 1) from well-characterized peridotite and pyroxenite xenoliths from Oahu, Hawaii. The peridotites are considered to be fragments of 90–100 Ma Pacific oceanic lithosphere or even ancient recycled mantle material within the Hawaiian mantle plume (Bizimis et al., 2007, 2004). The garnet pyroxenites are considered to be high-pressure cumulates from OIB-like melts that formed close to the lithosphere–asthenosphere boundary (60–90 km) (Bizimis et al., 2013, 2005; Sen et al., 2005, 2011), while some samples with majorite pseudomorphs (Keshav and Sen, 2001) and nanodiamonds (Wirth and Rocholl, 2003) potentially originated at depths >150 km. In this study, we use peridotite Fe isotope compositions to infer the Fe-isotope systematics of the peridotitic upper mantle and pyroxenites to explore the Fe-isotope systematics of mineralogically enriched

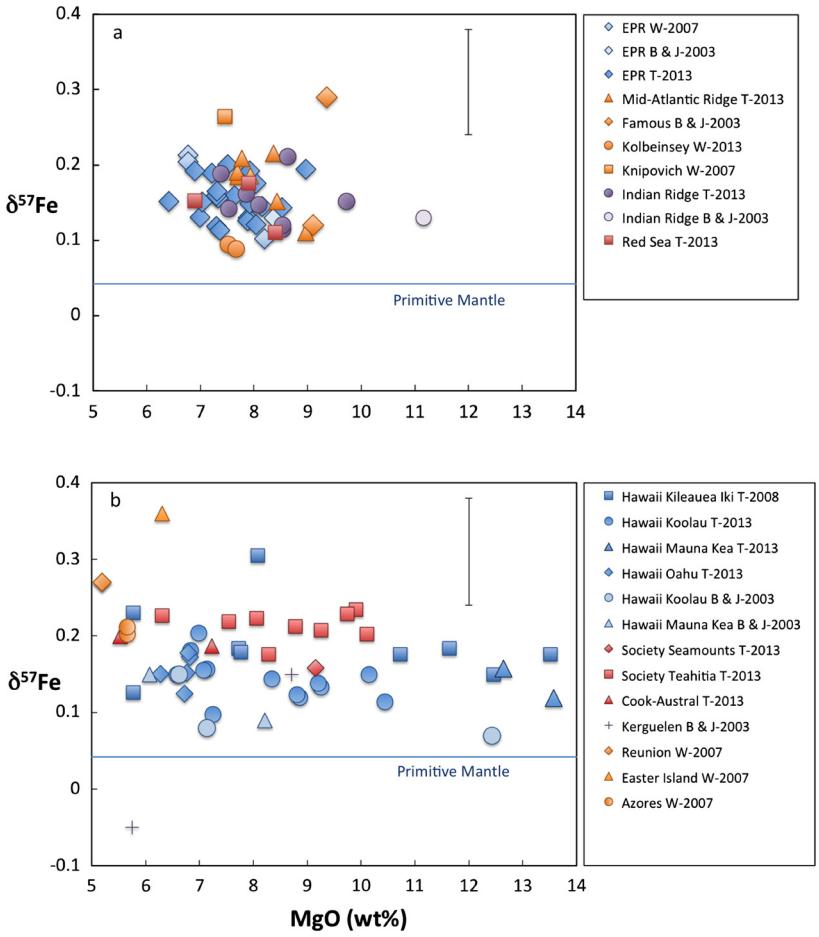

Fig. 2. Literature iron isotope data for MORB (a) (EPR, East Pacific Rise; MAR, Mid Atlantic Ridge) and OIB (b). Data sources and key to legend: W-2007 (Weyer and Ionov, 2007); W-2005 (Weyer et al., 2005); T-2013 (Teng et al., 2013); B & J – 2003 (Beard et al., 2003); T-2008 (Teng et al., 2008). The Fe isotope composition inferred for the PM (0.04‰) is shown as a horizontal line on both plots. Errors on isotopic composition are typically 0.02 to 0.09‰ and smaller than the overall variation in δ^{57}Fe observed (our 2 S.D. long term reproducibility is shown for reference as an error bar on this plot). Icelandic basalts (Schuessler et al., 2009) were not plotted as i) they sample both MORB-source and enriched mantle source regions ascribed to the Icelandic plume, which could make identifying differences in Fe-isotope systematics of MORB and OIB more difficult ii) they are comparatively fractionated, as detailed by (Schuessler et al., 2009). Samples <5.5 wt% and >14 wt% MgO were excluded to avoid magmatic fractionation (Schuessler et al., 2009) and olivine accumulation effects (Teng et al., 2008) respectively.

lithologies in the mantle, and we evaluate these results in the context of published Fe isotope data for MORB and OIB.

2. Materials and methods

2.1. Samples

The samples studied here are mantle xenoliths from the Salt Lake Crater (SLC) Pali and Kaau vents that belong to the Honolulu Volcanics series in Oahu, Hawaii, which are part of the rejuvenated or post-erosional stage of the Hawaiian volcanism (Clague and Frey, 1982; Ozawa et al., 2005; Sen et al., 2005). A location map is provided in Appendix A. In this study we focus on previously studied, well-characterized spinel lherzolite and garnet pyroxenite xenoliths (Bizimis et al., 2013, 2004, 2005; Sen et al., 2011) as well as some newly reported samples. The samples are from the Dale Jackson and Dean Presnall collections at the Smithsonian Institution. The peridotites are all spinel lherzolites with ~5–12 modal % clinopyroxene, and are fresh, free of serpentinization and visible melt infiltration (e.g. veins). The bulk rock Mg# (reconstructed from mineral abundance and compositions) vary from 0.89 to 0.90, ranging from fertile (McDonough and Sun, 1995) or Depleted Mantle (Salters and Stracke, 2004) compositions to more Mg-rich, and therefore more depleted values. The degree of melting experienced by the peridotites, as calculated from spinel Cr# (Hellebrand et al., 2001), ranges from ~1–12% (Table 1). Clinopyroxene and spinel Cr# and clinopyroxene HREE contents are all highly correlated (Bizimis et al., 2007), consistent with major and trace element equilibration between the primary mineral phases. All the clinopyroxenes from the samples reported here exhibit different degrees of light rare earth element (LREE) enrichment, with concave down to concave up chondrite-normalized REE patterns, consistent with variable refertilization by incompatible element enriched melts (Bizimis et al., 2007, 2004). Based on their combined major, trace element and Sr–Nd–Hf–Os isotope systematics, the Pali and Kaau peridotites are generally thought to represent comparatively unmodified parts of the Pacific lithosphere beneath Oahu (Bizimis et al., 2007, 2004; Sen et al., 1993). In contrast, the SLC peridotites have experienced, on average, a greater extent of melt depletion (e.g. higher pyroxene Mg# and Cr#), and re-enrichment (higher Na and LREE) relative to the Pali and Kaau peridotites. They have highly radiogenic Hf isotope (Bizimis et al., 2007, 2004; Salters and Zindler, 1995) and unradiogenic Os isotope compositions, with Re-depletion ages up to 2 Ga (Bizimis et al., 2007), which have been explained by a scenario in which these peridotites represent fragments of ancient (>1 Ga old) recycled lithosphere entrained as part of the upwelling Hawaiian plume.

The pyroxenites are classified as garnet–clinopyroxenites with 10–30 volume % garnet, >50% clinopyroxene (augite) and subordinate amounts of olivine, orthopyroxene, spinel and traces of

Table 1
Iron isotope data for Hawaiian peridotite and pyroxenite xenoliths.

	Peridotites						Pyroxenites			
	Pa 27	KAPS-36	77SL-405	77SL-466	77SL-341	77SL-402	77SL-594	77SL-601	77SL-582	NMNH-114954-20A
% cpx	10	10	5	12	10	10	84.7	70	70	82
% opx	25	28	25	24	20	28	5	0	0	0
% garnet	–	–	–	–	–	–	10	30	30	8
% olivine	63	60	68	63	68	60	–	–	–	–
% spinel	2	2	2	2	1	2	0.3	–	–	–
δ^{57}Fe cpx	0.16	0.12	−0.07	0.13	−0.21	−0.04	0.17	0.33	0.14	0.25
2 S.D.	0.03	0.04	0.09	0.06	0.07	0.05	0.06	0.03	0.02	0.01
δ^{56}Fe cpx	0.08	0.08	−0.04	0.07	−0.14	−0.03	0.12	0.23	0.09	0.16
2 S.D.	0.04	0.06	0.06	0.03	0.03	0.04	0.01	0.02	0.01	0.02
δ^{57}Fe opx	−0.09	0.12	−0.20	0.03	−0.08	−0.04				
2 S.D.	0.06	0.01	0.01	0.04	0.09	0.04				
δ^{56}Fe opx	−0.07	0.08	−0.13	0.04	−0.07	−0.02				
2 S.D.	0.02	0.04	0.01	0.02	0.06	0.02				
δ^{57}Fe ol	−0.07	0.15	−0.38	0.10	−0.21	0.00				
2 S.D.	0.03	0.06	0.06	0.04	0.04	0.02				
δ^{56}Fe ol	−0.06	0.09	−0.25	0.05	−0.15	−0.02				
2 S.D.	0.02	0.07	0.04	0.06	0.04	0.01				
δ^{57}Fe gt							0.15	0.21	0.04	0.03
2 S.D.							0.01	0.03	0.05	0.07
δ^{56}Fe gt							0.08	0.10	0.01	0.02
2 S.D.							0.01	0.06	0.02	0.03
δ^{57}Fe bulk	**−0.07**	**0.14**	**−0.34**	**0.09**	**−0.19**	**−0.01**	**0.17**	**0.27**	**0.10**	**0.21**
2 S.D.	**0.08**	**0.08**	**0.11**	**0.08**	**0.12**	**0.07**	**0.06**	**0.05**	**0.05**	**0.07**
δ^{56}Fe bulk	−0.06	0.09	−0.23	0.05	−0.14	−0.02	0.11	0.16	0.05	0.14
2 S.D.	0.05	0.10	0.07	0.06	0.08	0.05	0.01	0.06	0.02	0.04
Δ^{57}Fe cpx-ol	0.23	−0.02	0.31	0.03	0.01	−0.03				
2 S.D. prop	0.04	0.08	0.11	0.07	0.08	0.05				
Δ^{57}Fe cpx-opx	0.25	0.01	0.13	0.10	−0.13	0.00				
2 S.D. prop	0.07	0.05	0.09	0.07	0.11	0.06				
Δ^{57}Fe cpx-gt							0.02	0.13	0.11	0.22
2 S.D. prop							0.06	0.05	0.05	0.07
FeO^t bulk	8.69	8.49	8.52	8.22	8.22	8.66	7.44	8.00	7.74	7.29
Cr# bulk	0.08	0.06	0.17	0.07	0.13	0.11	0.00	0.00	0.01	0.00
Mg# bulk	0.89	0.89	0.90	0.90	0.90	0.89	0.75	0.76	0.79	0.73
% melting	1.5	1.5	12.3	2.4	9.3	5.8				
T (C)	1008	1012	1079	1041	1039	1046	1006	1236	1275	1283
εHf(cpx) ± 2	18.9 ± 0.8	11.8 ± 0.7	26.3 ± 1	19.3 ± 0.5	24.3 ± 0.7	28.3 ± 0.1	12.9 ± 0.2	15.4 ± 0.5	15.1 ± 0.8	14.3 ± 0.4

Mineral abbreviations: cpx, clinopyroxene; opx, orthopyroxene; ol, olivine; gt, garnet. Errors on Fe isotope measurements are 2 S.D. calculated for replicate analyses. Errors on bulk values are propagated using mineral errors and standard error propagation techniques. Iron isotope measurements followed protocols detailed in Methods. Bulk rock molar Mg# = Mg/(Fe + Mg) and Cr# = Al/(Cr + Al) values were calculated based on mineral modes and compositions from Bizimis et al. (2004, 2005) and new data generated as in those studies. Equilibration temperatures are taken from Bizimis et al. (2004, 2005) and peridotite and garnet pyroxenite pressures are assumed to be 18 and 25 kbar, respectively. Temperature data for samples 77SL-402, 77SL-594 and NMNH-114954-20A are calculated as in the previous studies. Hafnium isotope compositions are from Bizimis et al. (2004, 2005) with new data for samples 77SL-402, 77SL-594 and NMNH-114954-20A reported here (see Methods section). The epsilon notation refers to the deviation from chondritic Hf ($^{176}Hf/^{177}Hf = 0.282785$) in parts per 10,000. The degree of partial melting was calculated following Hellebrand et al. (2001).

phlogopite. Based on major and trace element modeling and their Sr, Nd, Hf, Pb, and Os isotope compositions they have been largely interpreted as high pressure (>2 GPa, >60 km) cumulates near the base of the Pacific lithosphere from melts similar to the Hawaiian alkali rejuvenated lavas (Bizimis et al., 2013, 2005; Keshav et al., 2007; Sen et al., 2010). Some samples display ilmenite exsolutions within garnet (including samples NMNH-114959-20A and 77SL-582 analyzed here), majorite pseudomorphs and nanodiamonds and probably initially crystallized at >5 GPa (>150 km) (Keshav and Sen, 2001; Keshav et al., 2007), deeper than the 80–90 km seismically defined base of the lithosphere beneath Oahu (Li et al., 2004). The radiogenic Hf and Nd isotopic compositions of the pyroxenites analyzed thus far (Bizimis et al., 2013, 2005), including the high pressure pyroxenite NMNH-114959-20A, place them at the depleted end of the OIB array, suggesting an origin from a depleted mantle source, distinct from the isotopically enriched "eclogitic" component inferred for the Hawaiian plume (Hauri, 1996; Huang and Frey, 2005).

2.2. Iron isotope analyses

Iron isotope analyses were carried out on hand-picked mineral grains, where individual sample aliquots consisted of 40–60 mineral grains between 120–200 μm in size. The samples were picked under ethanol using a binocular microscope avoiding crystals with obvious cracks, external alteration and mineral or fluid inclusions and were subsequently cleaned in ultrapure Millipore® 18.2 Ω water. Dissolution, iron purification and isotopic analyses were undertaken at Durham University using established procedures (Hibbert et al., 2012; Williams et al., 2012). Isotopic analyses were carried out on a multiple-collector inductively coupled plasma mass spectrometer (MC-ICPMS; Thermo Neptune) (Williams et al., 2012). Sample solutions consisted of 0.9 to 1.5 ppm Fe (different concentrations were chosen on different days according to instrument sensitivity) in 0.1M HNO_3, and instrumental mass bias was corrected for by sample–standard bracketing where the sample and standard Fe beam intensities (typically 35–40 V ^{56}Fe for a standard 10^{11} Ω resistor) were matched to 5%. Mass dependence, long-term reproducibility and accuracy were evaluated by analysis of an in-house FeCl salt standard ($\delta^{57}Fe = -1.06 \pm 0.07$‰; $\delta^{56}Fe = -0.71 \pm 0.06$‰ 2 S.D., $n = 35$) previously analyzed in other studies (Hibbert et al., 2012; Williams et al., 2012). The international rock standards BIR-1 (Icelandic basalt) and Nod-PI (Pacific ferromanganese nodule) were also analyzed over the course of this study (Table A.2). The mean Fe isotope compositions of these standards are: BIR-1, $\delta^{57}Fe = 0.082 \pm 0.01$‰; $\delta^{56}Fe = 0.062 \pm 0.01$‰

(2 S.D., $n = 6$), Nod-P1 $\delta^{57}Fe = -0.837 \pm 0.02‰$; $\delta^{56}Fe = -0.569 \pm 0.03‰$ (2 S.D., $n = 7$). The data for BIR-1 are in excellent agreement with earlier studies (Hibbert et al., 2012; Millet et al., 2012; Weyer et al., 2005) and the results for Nod-PI fall within the median of literature values which range from $\delta^{56}Fe = -0.67$ to $\delta^{56}Fe = -0.49‰$ (Asael et al., 2013; Gagnevin et al., 2012). Iron yields were quantitative and chemistry blanks were <0.5 ng Fe, negligible compared to the quantities of sample Fe (>300 μg) processed.

2.3. Hafnium isotope analyses

New hafnium isotope data on clinopyroxene from samples 77SL-402 and 77SL-594 were obtained at the Center for Elemental Mass Spectrometry, University of South Carolina, on a Thermo Neptune MC-ICPMS using established chemical procedures (Bizimis et al., 2007, 2013), and are reported here for data completeness. The JMC Hf standard yielded values of $^{176}Hf/^{177}Hf = 0.282142 \pm 5$ (2 S.D., $n = 10$; 20 ng runs), and all ratios are reported relative to $^{176}Hf/^{177}Hf = 0.282160$ for this standard. Hafnium blanks were <50 pg. Hafnium isotope data reported in Table 1 in the epsilon notation relative to a chondritic $^{176}Hf/^{177}Hf = 0.282785$.

3. Results

Bulk peridotite $\delta^{57}Fe$ values (Table 1 and Fig. 3) were calculated from mineral separate data, mineral modal abundances and Fe concentrations (Table 1) and range from $-0.34 \pm 0.11‰$ to $0.14 \pm 0.08‰$; bulk pyroxenite $\delta^{57}Fe$ varies from $0.10 \pm 0.05‰$ to $0.27 \pm 0.05‰$ (all errors are 2 S.D., propagated using sum-of-squares and the 2 S.D. errors in Table 1). These differences are also evident at the mineral scale as peridotite clinopyroxene $\delta^{57}Fe$ values range from $-0.21 \pm 0.07‰$ to $0.16 \pm 0.03‰$, whereas pyroxenite clinopyroxenes have heavier $\delta^{57}Fe$ values of $0.14 \pm 0.02‰$ to $0.33 \pm 0.03‰$. Apparent inter-mineral fractionation factors are also presented in Table 1 and Fig. 4. In the peridotites, clinopyroxene is either isotopically heavier, or within error identical to coexisting olivine. A similar pattern is observed for clinopyroxene–orthopyroxene pairs with the exception of sample 77SL-341, where orthopyroxene displays a heavier $\delta^{57}Fe$ value relative to clinopyroxene. In the pyroxenites, clinopyroxenes display $\delta^{57}Fe$ values that are heavier or, in one case (sample 77SL-594) within error of coexisting garnet. While the overall tendency of clinopyroxene to display heavy $\delta^{57}Fe$ values with respect to olivine, orthopyroxene and garnet is consistent with theory and studies of natural peridotites, pyroxenites and eclogites (Beard and Johnson, 2004; Weyer and Ionov, 2007; Williams et al., 2009, 2005), the variability observed in calculated intra-mineral fractionation factors (Table 1) is not consistent with isotopic equilibrium over the narrow range of equilibration temperatures inferred for these samples (Table 1). This variation could reflect late-stage Fe-isotope redistribution between minerals, or potentially melt–rock reaction and diffusion processes. However, no systematic correlations between mineral fractionation factors or other mineral or whole-rock chemical parameters are evident, suggesting that the processes which induced mineral isotopic disequilibria did not modify the Fe isotope compositions of the bulk samples. An alternative scenario could be the incorporation of isotopically light xenocrystic olivine, which is known to be present in the Hawaiian system as a function of fractional crystallization processes (Teng et al., 2008). This process would increase measured clinopyroxene–olivine fractionation factors and reduce bulk $\delta^{57}Fe$, and could potentially account for the light olivine $\delta^{57}Fe$ values observed in 77SL-405, which also has an elevated bulk MgO content relative to the other SLC peridotites.

4. Discussion

4.1. Peridotite Fe isotope compositions and the role of melt extraction

Strong negative correlations exist between bulk peridotite $\delta^{57}Fe$ and indicators of melt extraction where the most depleted peridotites (i.e. highest spinel and bulk rock Cr#, lowest clinopyroxene Al-contents; Fig. 3a, b, c) display the lightest $\delta^{57}Fe$ values. A negative array is also present between $\delta^{57}Fe$ and hafnium isotopes (εHf; Fig. 3d), a radiogenic isotopic system that records the time-integrated fractionation of Hf from Lu during partial melting and which has been shown to be generally resistant to overprint by mantle metasomatism (Bizimis et al., 2004; Lazarov et al., 2012; Stracke et al., 2011). While Fe stable isotopes do not record temporal information, the observed correlation between Fe isotopes and Hf isotopes does suggest that the samples with the greatest radiogenic isotope signatures of time-integrated melt extraction are also the most isotopically fractionated in terms of Fe. One possibility is that Fe and Hf isotopes record the same partial melting events. However, such a direct link is not supported by the melting models in Section 1.2 coupled with the estimated degree of melt extraction (Hellebrand et al., 2001) recorded by the peridotites, which are not sufficient to generate the observed range in peridotite $\delta^{57}Fe$. Other explanations for the range in peridotite $\delta^{57}Fe$ must therefore be considered.

While hydrothermal alteration and seawater contamination are processes that can influence the trace element and radiogenic isotope budgets of oceanic basalts and abyssal peridotites (Burton et al., 2012), the samples studied here are pristine with little evidence of post-magmatic alteration (Bizimis et al., 2004, 2005; Sen et al., 2011). Moreover, composite oceanic crust (Rouxel et al., 2003) and sheeted dyke samples (Williams et al., 2009) display $\delta^{57}Fe$ values within error of mean MORB, suggesting that these processes have little impact on Fe isotopes. Incorporation of xenocrystic olivine, discussed in the previous section, could in principle contribute to the low $\delta^{57}Fe$ value of 77SL-405, but it is not clear how this process would generate correlations between $\delta^{57}Fe$ and Hf isotopes. Metasomatic refertilisation, and melt-peridotite reaction are processes that can explain the Hf-decoupling from Sr and Nd isotopes and the elevated light rare earth element (LREE) abundances of the Oahu peridotites (Bizimis et al., 2004). However these mechanisms, without any additional stable isotope fractionation process, cannot explain the range in peridotite $\delta^{57}Fe$ as relationships between $\delta^{57}Fe$ and Nd and Sr isotopes or Na and LREE contents are absent. Furthermore, mass balance calculations show that unfeasibly large ratios of melt to peridotite (91:9, for a melt with a $\delta^{57}Fe$ value of ~0.15‰ and the peridotite 77SL-405 with the lowest bulk rock $\delta^{57}Fe$) are required, which are inconsistent with the high Mg#'s and Cr#'s of the peridotites (Table 1).

One means of reconciling the relatively large variation in peridotite $\delta^{57}Fe$ and the correlations between peridotite $\delta^{57}Fe$ and indicators of partial melt extraction could be derivation from a $\delta^{57}Fe$-heterogeneous mantle. In this scenario, the correlations between peridotite $\delta^{57}Fe$, εHf and proxies for melt extraction indicate that the processes responsible for Fe-isotope heterogeneity must be magmatic in nature. Distinct mantle source regions have previously been invoked to explain the elemental (Dasgupta et al., 2010; Hirschmann and Stolper, 1996; Prytulak and Elliott, 2007) and radiogenic isotope signatures (Chauvel et al., 1992; Hofmann, 1997; Salters et al., 2011; Stracke et al., 2005, 1999; White and Hofmann, 1982; Workman et al., 2004) of many oceanic basalt suites. At least two modified mantle source components in addition to primitive mantle (PM; 0.04‰; Dauphas et al., 2009) must be invoked in order to explain the peridotite $\delta^{57}Fe$ arrays. In this scenario, a long-lived depleted source with radiogenic εHf and light $\delta^{57}Fe$ would be required to account for the light $\delta^{57}Fe$ val-

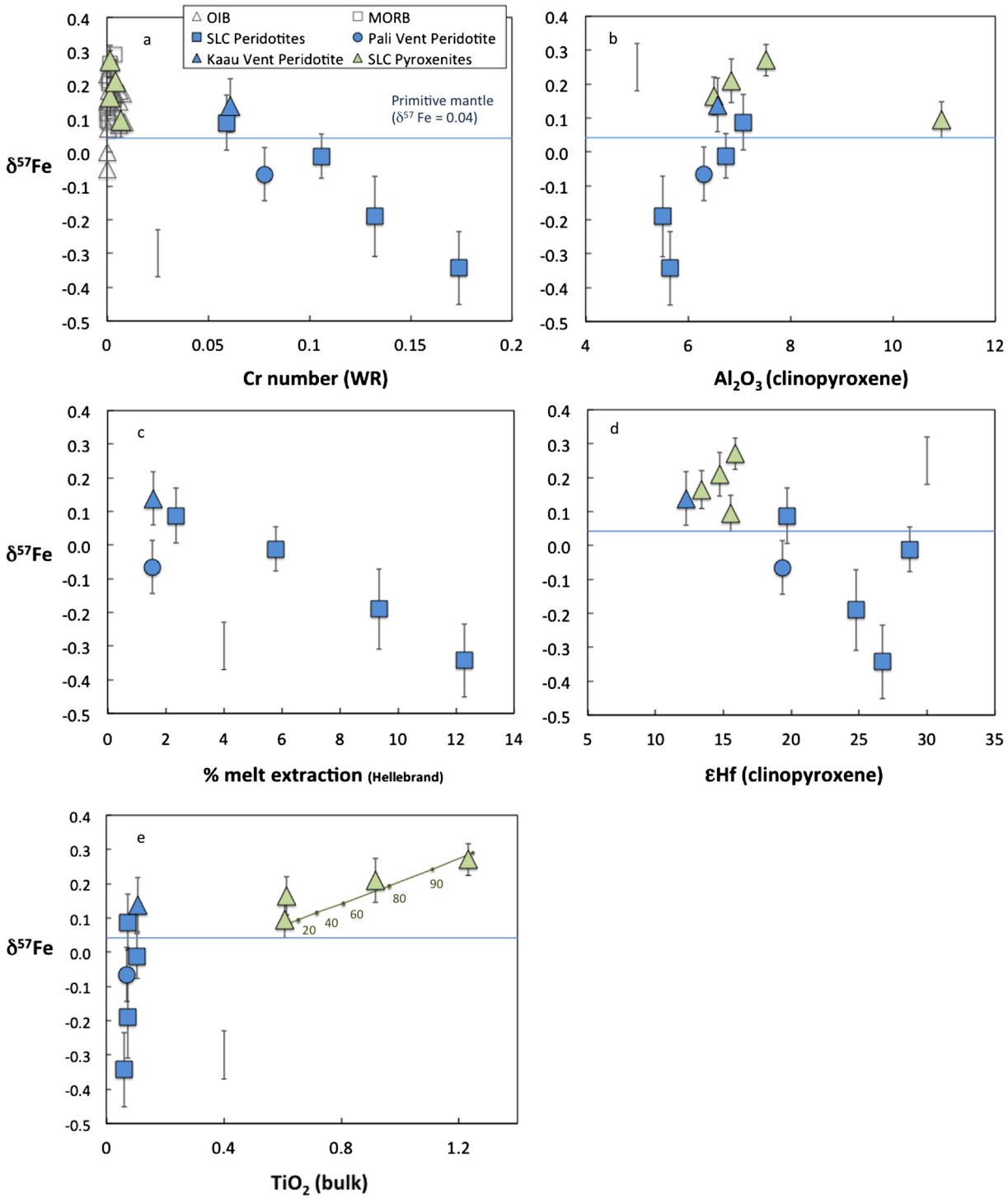

Fig. 3. a) Bulk sample δ^{57}Fe versus Cr# (molar Cr/Cr+Al) SLC: Salt Lake Crater. R^2 values for peridotite correlations: 0.90 (all); 0.98 (SLC). Bulk sample δ^{57}Fe and elemental abundances were calculated using mineral modes, Fe contents and isotopic compositions in Table 1. Bulk δ^{57}Fe errors were calculated using standard propagation techniques and given 2 S.D. errors. As detailed in the main text, the long-term reproducibility is 0.07‰ for the in-house standard and is shown as an error bar in all panels. **b)** Bulk sample δ^{57}Fe versus clinopyroxene Al_2O_3 (wt%). Peridotite array R^2 values: 0.84 (all); 0.84 (SLC). **c)** Bulk sample δ^{57}Fe versus % partial melt extraction (Hellebrand et al., 2001). R^2 values: 0.81 (all); 0.98 (SLC). **d)** Bulk sample δ^{57}Fe versus clinopyroxene hafnium isotope compositions. **e)** Bulk sample δ^{57}Fe versus TiO_2 (wt%). Model curve shows the evolution of cumulate residues in equilibrium with fractional melts generated from an initial melt with δ^{57}Fe = 0.15‰ and TiO_2 = 1.96 wt%. Tick marks show % melt removed. The model uses a bulk garnet pyroxenite Ti partition coefficient of 0.31 (Johnson, 1998) and was fitted to the data by adjusting the δ^{57}Fe of the initial melt and $\alpha_{\text{melt-residue}}$. The optimal value of $\alpha_{\text{melt-residue}}$ was 1.00007 (0.07‰). The calculated TiO_2 content of the initial melt is 1.96 wt%, assuming equilibrium with the most primitive pyroxenite (Bizimis et al., 2005; Sen et al., 2011), and is similar to TiO_2 contents displayed by Hawaiian OIB, which may reflect the small amounts of altered oceanic crust in their source regions (Prytulak and Elliott, 2007). The δ^{57}Fe value of this primitive melt is estimated to be 0.15‰, within error of mean OIB, MORB and oceanic crust. The large degree of fractional crystallization required to generate the full range of pyroxenite TiO_2 contents could also be indicative of source TiO_2 heterogeneity, but this does not affect the overall conclusions drawn here.

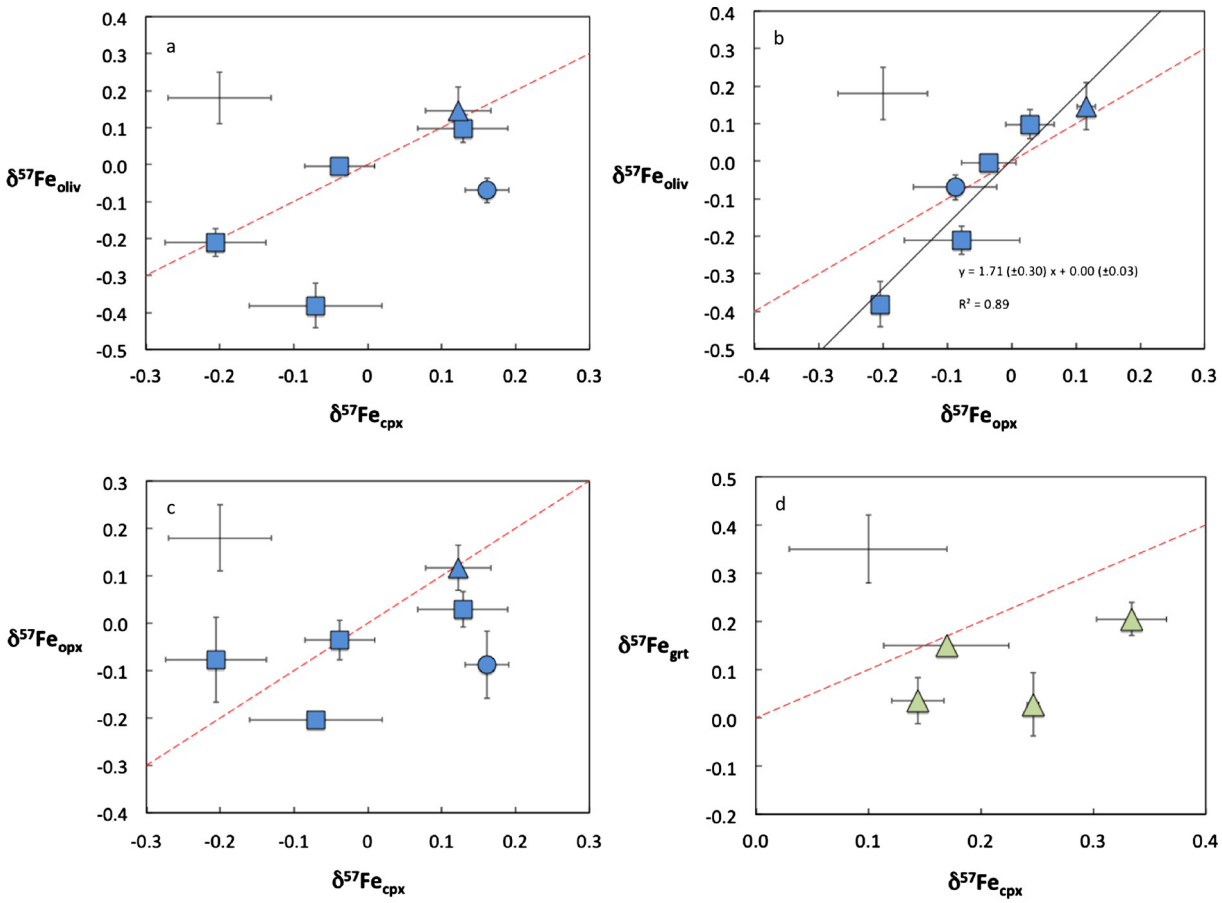

Fig. 4. Mineral–mineral Fe isotope plots for clinopyroxene vs olivine (a), orthopyroxene vs olivine (b), clinopyroxene vs orthopyroxene (c) and clinopyroxene vs garnet (d). Symbols are as in Fig. 3. The long-term reproducibility for δ^{57}Fe is shown as an error cross on all plots. Dotted curves show a reference line with a slope of 1. The linear regression shown in (b) was calculated using standard least-squares fitting procedures; errors are 95% confidence.

ues and radiogenic εHf of the most depleted samples. If 77SL-405 is excluded from the data array and the sample 77SL-341 (bulk $\delta^{57}\text{Fe} = -0.19 \pm 0.12‰$; $\varepsilon\text{Hf} = 24.2$) taken as the most depleted endmember, the δ^{57}Fe value of this source is required to be $\sim -0.15‰$ (from the models in Section 1.2, allowing for a source-residue fractionation of 0.04‰ at 30% melt extraction), extremely similar to that inferred for the Gorgona komatiites (Hibbert et al., 2012).

Because the models in Section 1.2 demonstrate that single-stage melt extraction from a BSE with an assumed δ^{57}Fe value of 0.04‰ cannot create strongly fractionated residues, this source region must have acquired this low δ^{57}Fe value either through multiple phases of melt extraction or a combination of processes including melt–rock reaction and melt percolation. Experimental studies of Fe isotope fractionation during partial melting, in both spinel and garnet facies, coupled with experiments simulating the effects of percolation and melt–rock reaction processes are required to test and refine these hypotheses.

At the high-δ^{57}Fe end of the peridotite array, the peridotite KAPS-36 ($\delta^{57}\text{Fe}$ $0.14 \pm 0.08‰$; Table 1) has a relatively low spinel Cr#, low bulk Mg# and slightly LREE enriched clinopyroxene chondrite-normalized REE patterns (Bizimis et al., 2004), all of which are indicative of derivation, via minimal levels of melt extraction, from relatively fertile mantle. The heavy δ^{57}Fe value of the peridotite KAPS-36, which is similar to mean MORB or OIB, indicates derivation from a source with a similar δ^{57}Fe value, as the models discussed in Section 1.2 show that the δ^{57}Fe values of melting residues at low degrees of melting are almost indistinguishable from the initial source. However, a source region with a δ^{57}Fe value of $\sim$0.14‰ cannot be created by mixing mantle melts (FeO = 8.10 wt%; $\delta^{57}\text{Fe} \sim 0.15‰$, assumed to be similar to MORB or OIB) and PM (FeO = 8.07 wt%; $\delta^{57}\text{Fe} \sim 0.04‰$), as unrealistic melt–rock ratios (92:8) are needed. A similar argument applies to mixtures of mantle peridotite and altered oceanic crust or oceanic sediments as these have δ^{57}Fe values within error of mean MORB (Rouxel et al., 2003), or, in the case of ferromanganese sediments, extremely light δ^{57}Fe values ($<-0.6‰$) (Levasseur et al., 2004). An additional means of generating mantle source components with heavy δ^{57}Fe values is therefore required.

4.2. Iron isotopes in the Oahu pyroxenite xenoliths and the formation of enriched mantle lithologies

The pyroxenites display δ^{57}Fe values up to $0.27 \pm 0.05‰$ and may represent an analogue for the heavy δ^{57}Fe mantle source components discussed above. Positive correlations exist between pyroxenite δ^{57}Fe and TiO_2 at the bulk rock and mineral level (Fig. 3), which likely reflect isotopic fractionation and the concentration of heavy δ^{57}Fe in evolved melts (Schuessler et al., 2009; Teng et al., 2008) and hence in the cumulates derived from these melts. A model for fractional crystallization and the evolution of cumulate residues is shown in Fig. 3; the δ^{57}Fe value of the initial melt is estimated to be 0.15‰, within error of mean OIB, MORB and altered oceanic crust. The calculated TiO_2 content of the initial melt is 1.96 wt%, assuming equilibrium with the most primitive pyroxenite (Bizimis et al., 2005; Sen et al., 2011), similar to the TiO_2 contents displayed by alkali rejuvenated stage Hawaiian lavas (Clague and Frey, 1982; Garcia et al., 2010), the presumed parental melt of these pyroxenites (Bizimis et al., 2013).

Pyroxenite cumulate residues (as well as evolved melts) generated by high-pressure basaltic magma fractionation therefore appear to possess heavy δ^{57}Fe signatures and high incompatible element concentrations. Therefore, pyroxenite cumulate components, irrespective of their origin, could contribute to the level of Fe-isotope heterogeneity observed in MORB and OIB source regions. For example, a source region with a δ^{57}Fe value of ~0.14‰, such as that required to generate the KAPS-36 peridotite, could be formed through a 55:45 mixture of cumulate pyroxenite melt to unmelted mantle peridotite (60% cumulate melt as modeled in Fig. 3, δ^{57}Fe = 0.21‰, peridotite δ^{57}Fe = 0.04‰, for simplicity both peridotite and pyroxenite melt are assumed to have the same FeO content of 8 wt%). This scenario is broadly consistent with the relatively fertile nature of the KAPS-36 peridotite, where the strong nature of LREE enrichment that such metasomatism would generate is then moderated by subsequent episode(s) of minor melt extraction.

4.3. Evidence for Fe-isotope heterogeneity in the mantle source regions of MORB and OIB

Multiple mantle source regions with distinct δ^{57}Fe are also required to explain the variation in MORB and OIB δ^{57}Fe. Considerable variability exists in the Fe isotope composition of fresh MORB and OIB (Fig. 2), which is not readily explained by magmatic differentiation or post-magmatic processes. For example, at a comparatively narrow range of MgO (6.4–11.2 wt%) MORB δ^{57}Fe ranges from 0.09 to 0.29‰, a range far greater than that predicted by any melting model. At a similar range of MgO contents (5.5–13.6 wt%), OIB δ^{57}Fe varies from −0.05 to 0.36‰. If Hawaiian OIB are considered alone, the extent of δ^{57}Fe variation is marginally reduced (δ^{57}Fe ranges from 0.07 to 0.31‰) but is still greater than the extent of isotopic variation predicted by the melting models in Section 1.2 (~0.03‰ for 2–20% partial melting).

Interestingly, OIB from the Cook-Austral and Society islands, which represent type examples of HIMU (high-μ, high ^{238}U/^{204}Pb; ^{206}Pb/^{204}Pb > 20.5, ^{87}Sr/^{86}Sr < 0.703) (Stracke et al., 2005) and EM2 OIB (enriched mantle; high ^{87}Sr/^{86}Sr) (Chauvel et al., 1992), respectively, have particularly heavy mean δ^{57}Fe values (0.21 ± 0.05‰ 2 S.D., n = 10, MgO 6.3–10.1 wt% and 0.19 ± 0.02‰ 2 S.D., n = 2, respectively, MgO 5.5–7.3 wt%) relative to other OIB. Student's t-tests demonstrate that this difference in mean δ^{57}Fe between Society and Hawaiian OIB (0.15 ± 0.09‰ 2 S.D., n = 34, MgO 5.8–13.6 wt%) is resolvable at the 95% confidence level, even when samples from Ko'olau, which define a subtlety lighter mean δ^{57}Fe (0.14 ± 0.07‰ 2 S.D., n = 13, MgO 6.3–10.1 wt%) than other Hawaiian OIB (Teng et al., 2013) are omitted from the Hawaiian dataset (Hawaii without Ko'olau: 0.17 ± 0.09‰ 2 S.D., n = 18, respectively, MgO 5.8–13.6 wt%). While the radiogenic Pb and Sr isotope compositions of EM2 and HIMU have been linked with recycled components such as subduction modified, low-Pb oceanic crust (HIMU) and terrigenous sediments (EM2) (Hofmann, 1997), these components do not have Fe isotope compositions significantly different to that of mean MORB (Rouxel et al., 2003) and therefore cannot explain the heavy δ^{57}Fe values of Society and Cook-Austral OIB. However, our data suggest that the process of pyroxenite cumulate formation from fractionated mafic melts (irrespective of their origin) can generate enriched mantle mineralogies and associated melts with heavy δ^{57}Fe values and our models demonstrate that pyroxenite source lithologies will generate melts with heavier δ^{57}Fe values than those from olivine-bearing sources under similar conditions. For example, oceanic basalts with δ^{57}Fe values of ~0.18‰ can be accounted for by a 70:30 mixture of 10% lherzolite melt and 20% garnet pyroxenite melt (both modeled in Section 1.2; a higher melting degree is assumed for the pyroxenite component given the greater melt productivity of that lithology), OIB with heavier δ^{57}Fe values of ~0.22‰ can be accounted for by a 30:70 mixture of 10% lherzolite melt and 20% garnet pyroxenite melt, or, if it assumed that such OIB represent smaller overall melting degrees, by a 40:60 mixture of 5% lherzolite melt and 10% garnet pyroxenite melt. In these calculations, the FeO contents of both endmembers are assumed to be equal; given the tendency of pyroxenites to have generally higher FeO contents relative to depleted peridotitic components this means that if anything, the amount of pyroxenite melt required is slightly overestimated. Hence, the presence of pyroxenite in mantle source regions is a viable mechanism for explaining the heavy δ^{57}Fe values of the Society and Cook-Austral OIB, and potentially places direct constraints on the mineralogy of the HIMU and EM2 mantle components themselves.

5. Conclusions

Iron stable isotopes are a powerful new tracer for detecting mineralogically distinct components in the source regions of oceanic basalts. Depleted peridotite and pyroxenite lithologies display contrasting Fe isotope signatures that correlate with elemental and radiogenic isotope tracers of magmatic processes. The light Fe isotope compositions of the peridotites are considered to arise through melt extraction, whereas the heavy δ^{57}Fe signatures of the pyroxenites reflect fractional crystallization processes near the base of the oceanic lithosphere. The absence of correlations between Fe isotopes and indices of metasomatism provides evidence that Fe isotopes are highly resistant to metasomatic overprinting.

Melting models cannot explain the level of Fe-isotope variation observed in MORB and OIB. We conclude that the source regions of both MORB and OIB are heterogeneous in terms of mineralogy and Fe isotopes. The heavy δ^{57}Fe values of OIB suites such as Society and Cook-Austral are indicative of pyroxenite components in their mantle source, while the low δ^{57}Fe values of the most depleted peridotites provide strong new evidence for the presence of highly depleted domains in the mantle. Because the latter material is so refractory, it is not widely sampled in most basalts (Salters et al., 2011), with the exception of those generated by exceptionally large degrees of partial melting, such as komatiites (Hibbert et al., 2012) and boninites (Dauphas et al., 2009), which display light δ^{57}Fe values relative to MORB and OIB. Iron isotope studies of large-degree partial melts and depleted peridotites may thus reveal the melt depletion and enrichment history of the convecting upper mantle.

Acknowledgements

The authors would like to thank Joel Baker, Kevin Burton, Karsten Haase, Ian Parkinson, Frank Poitrasson and Pete Tollan for constructive discussions. Fang-Zhen Teng is acknowledged for helpful discussions and providing access to new OIB Fe isotope data prior to its publication. Geoff Nowell is thanked for his invaluable and dedicated technical support. Stefan Weyer and an anonymous reviewer are thanked for their constructive and helpful reviews and Tim Elliott, as editor, for his numerous suggestions, which truly helped us improve this paper. Helen Williams is funded by NERC (Advanced Fellowship NE/F014295/1) and the European Research Council (ERC Starting Grant 306655 "Habitable-Planet"). Michael Bizimis is funded by NSF (NSF-OCE 1129280).

Appendix A. Supplementary material

Supplementary material related to this article can be found online at http://dx.doi.org/10.1016/j.epsl.2014.07.033.

References

Allègre, C.J., Turcotte, D.L., 1986. Implications of a two component marble-cake mantle. Nature 323, 123–127.

Asael, D., Tissot, F.L.H., Reinhard, C.T., Rouxel, O., Dauphas, N., Lyons, T.W., Ponzevera, E., Liorzou, C., Chéron, S., 2013. Coupled molybdenum, iron and uranium stable isotopes as oceanic paleoredox proxies during the Paleoproterozoic Shunga Event. Chem. Geol. 362, 193–210.

Beard, B.L., Johnson, C.M., 2004. Inter-mineral Fe isotope variations in mantle-derived rocks and implications for the Fe geochemical cycle. Geochim. Cosmochim. Acta 68, 4727–4743.

Beard, B.L., Johnson, C.M., Skulan, J.L., Nealson, K.H., Cox, L., Sun, H., 2003. Application of Fe isotopes to tracing the geochemical and biological cycling of Fe. Chem. Geol. 195, 87–117.

Bizimis, M., Sen, G., Salters, V.J.M., 2004. Hf–Nd isotope decoupling in the oceanic lithosphere: constraints from spinel peridotites from Oahu, Hawaii. Earth Planet. Sci. Lett. 217, 43–58.

Bizimis, M., Sen, G., Salters, V.J.M., Keshav, S., 2005. Hf–Nd–Sr isotope systematics of garnet pyroxenites from Salt Lake Crater, Oahu, Hawaii: evidence for a depleted component in Hawaiian volcanism. Geochim. Cosmochim. Acta 69, 2629–2646.

Bizimis, M., Griselin, M., Lassiter, J.C., Salters, V.J.M., Sen, G., 2007. Ancient recycled mantle lithosphere in the Hawaiian plume: osmium–hafnium isotopic evidence from peridotite mantle xenoliths. Earth Planet. Sci. Lett. 257, 259–273.

Bizimis, M., Salters, V.J., Garcia, M.O., Norman, M.D., 2013. The composition and distribution of the rejuvenated component across the Hawaiian plume: Hf–Nd–Sr–Pb isotope systematics of Kaula lavas and pyroxenite xenoliths. Geochem. Geophys. Geosyst. 14, 4458–4478.

Burton, K.W., Cenki-Tok, B., Mokadem, F., Harvey, J., Gannoun, A., Alard, O., Parkinson, I.J., 2012. Unradiogenic lead in Earth's upper mantle. Nat. Geosci. 5, 570–573.

Chauvel, C., Hofmann, A.W., Vidal, P., 1992. HIMU EM – the French–Polynesian Connection. Earth Planet. Sci. Lett. 110, 99–119.

Clague, D.A., Frey, F.A., 1982. Petrology and trace-element geochemistry of the Honolulu Volcanics, Oahu – implications for the Oceanic Mantle Below Hawaii. J. Petrol. 23, 447–504.

Craddock, P.R., Warren, J.M., Dauphas, N., 2013. Abyssal peridotites reveal the near-chondritic Fe isotopic composition of the Earth. Earth Planet. Sci. Lett. 365, 63–76.

Dasgupta, R., Jackson, M.G., Lee, C.-T.A., 2010. Major element chemistry of ocean island basalts: conditions of mantle melting and heterogeneity of mantle source. Earth Planet. Sci. Lett. 289, 377–392.

Dauphas, N., Craddock, P.R., Asimow, P.D., Bennett, V.C., Nutman, A.P., Ohnenstetter, D., 2009. Iron isotopes may reveal the redox conditions of mantle melting from Archean to Present. Earth Planet. Sci. Lett. 288, 255–267.

Downes, H., 2007. Origin and significance of spinel and garnet pyroxenites in the shallow lithospheric mantle: ultramafic massifs in orogenic belts in Western Europe and NW Africa. Lithos 99, 1–24.

Elliott, T., Blichert-Toft, J., Heumann, A., Koetsier, G., Forjaz, V., 2007. The origin of enriched mantle beneath Sao Miguel, Azores. Geochim. Cosmochim. Acta 71, 219–240.

Gagnevin, D., Boyce, A., Barrie, C., Menuge, J., Blakeman, R., 2012. Zn, Fe and S isotope fractionation in a large hydrothermal system. Geochim. Cosmochim. Acta 88, 183–198.

Garcia, M.O., Swinnard, L., Weis, D., Greene, A.R., Tagami, T., Sano, H., Gandy, C.E., 2010. Petrology, Geochemistry and Geochronology of Kaua'i Lavas over 4.5 Myr: implications for the Origin of Rejuvenated Volcanism and the Evolution of the Hawaiian Plume. J. Petrol. 51, 1507–1540.

Gurenko, A.A., Sobolev, A.V., Hoernle, K.A., Hauff, F., Schmincke, H.-U., 2009. Enriched, HIMU-type peridotite and depleted recycled pyroxenite in the Canary plume: a mixed-up mantle. Earth Planet. Sci. Lett. 277, 514–524.

Hauri, E.H., 1996. Major-element variability in the Hawaiian mantle plume. Nature 382, 415–419.

Hauri, E.H., Lassiter, J.C., DePaolo, D.J., 1996. Osmium isotope systematics of drilled lavas from Mauna Loa, Hawaii. J. Geophys. Res., Solid Earth 1978–2012 (101), 11793–11806.

Heimann, A., Beard, B.L., Johnson, C.M., 2008. The role of volatile exsolution and subsolidus fluid/rock interactions in producing high Fe-56/Fe-54 ratios in siliceous igneous rocks. Geochim. Cosmochim. Acta 72, 4379–4396.

Hellebrand, E., Snow, J.E., Dick, H.J.B., Hofmann, A.W., 2001. Coupled major and trace elements as indicators of the extent of melting in mid-ocean-ridge peridotites. Nature 410, 677–681.

Herzberg, C., 2004. Partial crystallization of mid-ocean ridge basalts in the crust and mantle. J. Petrol. 45, 2389–2405.

Hibbert, K.E.J., Williams, H.M., Kerr, A.C., Puchtel, I.S., 2012. Iron isotopes in ancient and modern komatiites: evidence in support of an oxidised mantle from Archean to present. Earth Planet. Sci. Lett. 321, 198–207.

Hirschmann, M.M., Stolper, E.M., 1996. A possible role for garnet pyroxenite in the origin of the "garnet signature" in MORB. Contrib. Mineral. Petrol. 124, 185–208.

Hofmann, A.W., 1997. Mantle geochemistry: the message from oceanic volcanism. Nature 385, 219–229.

Hofmann, A.W., White, W.M., 1982. Mantle plumes from ancient oceanic-crust. Earth Planet. Sci. Lett. 57, 421–436.

Huang, S., Frey, F.A., 2005. Recycled oceanic crust in the Hawaiian Plume: evidence from temporal geochemical variations within the Koolau Shield. Contrib. Mineral. Petrol. 149, 556–575.

Humayun, M., Qin, L., Norman, M.D., 2004. Geochemical evidence for excess iron in the mantle beneath Hawaii. Science 306, 91–94.

Ionov, D.A., Hofmann, A.W., 2007. Depth of formation of subcontinental off-craton peridotites. Earth Planet. Sci. Lett. 261, 620–634.

Jackson, M.G., Dasgupta, R., 2008. Compositions of HIMU, EM1, and EM2 from global trends between radiogenic isotopes and major elements in ocean island basalts. Earth Planet. Sci. Lett. 276, 175–186.

Johnson, K.T., 1998. Experimental determination of partition coefficients for rare earth and high-field-strength elements between clinopyroxene, garnet, and basaltic melt at high pressures. Contrib. Mineral. Petrol. 133, 60–68.

Keshav, S., Sen, G., 2001. Majoritic garnets in Hawaiian xenoliths: preliminary results. Geophys. Res. Lett. 28, 3509–3512.

Keshav, S., Gudfinnsson, G.H., Sen, G., Fei, Y., 2004. High-pressure melting experiments on garnet clinopyroxenite and the alkalic to tholeiitic transition in ocean-island basalts. Earth Planet. Sci. Lett. 223, 365–379.

Keshav, S., Sen, G., Presnall, D.C., 2007. Garnet-bearing xenoliths from Salt Lake crater, Oahu, Hawaii; high-pressure fractional crystallization in the oceanic mantle. J. Petrol. 48, 1681–1724.

Klein, E.M., Langmuir, C.H., 1987. Global correlations of ocean ridge basalt chemistry with axial depth and crustal thickness. J. Geophys. Res., Solid Earth 92, 8089–8115.

Kogiso, T., Hirschmann, M.M., 2006. Partial melting experiments of bimineralic eclogite and the role of recycled mafic oceanic crust in the genesis of ocean island basalts. Earth Planet. Sci. Lett. 249, 188–199.

Kogiso, T., Hirschmann, M.M., Frost, D.J., 2003. High-pressure partial melting of garnet pyroxenite: possible mafic lithologies in the source of ocean island basalts. Earth Planet. Sci. Lett. 216, 603–617.

Lassiter, J.C., Hauri, E.H., 1998. Osmium-isotope variations in Hawaiian lavas: evidence for recycled oceanic lithosphere in the Hawaiian plume. Earth Planet. Sci. Lett. 164, 483–496.

Lazarov, M., Brey, G.P., Weyer, S., 2012. Evolution of the South African mantle—a case study of garnet peridotites from the Finsch diamond mine (Kaapvaal craton); Part 2: multiple depletion and re-enrichment processes. Lithos 154, 210–223.

Levasseur, S., Frank, M., Hein, J.R., Halliday, A.N., 2004. The global variation in the iron isotope composition of marine hydrogenetic ferromanganese deposits: implications for seawater chemistry? Earth Planet. Sci. Lett. 224, 91–105.

Li, X., Kind, R., Yuan, X., Wolbern, I., Hanka, W., 2004. Rejuvenation of the lithosphere by the Hawaiian plume. Nature 427, 827–829.

Liu, C.-Z., Snow, J.E., Hellebrand, E., Bruegmann, G., von der Handt, A., Buechl, A., Hofmann, A.W., 2008. Ancient, highly heterogeneous mantle beneath Gakkel ridge, Arctic Ocean. Nature 452, 311–316.

Lundstrom, C., Sampson, D., Perfit, M., Gill, J., Williams, Q., 1999. Insights into mid-ocean ridge basalt petrogenesis: U-series disequilibria from the Siqueiros Transform, Lamont Seamounts, and East Pacific Rise. J. Geophys. Res. 104, 13035–13048.

McDonough, W.F., Sun, S.-S., 1995. The composition of the Earth. Chem. Geol. 120, 223–253.

Millet, M.-A., Baker, J.A., Payne, C.E., 2012. Ultra-precise stable Fe isotope measurements by high resolution multiple-collector inductively coupled plasma mass spectrometry with a ^{57}Fe–^{58}Fe double spike. Chem. Geol. 304, 18–25.

Niu, Y.L., O'Hara, M.J., 2003. Origin of ocean island basalts: a new perspective from petrology, geochemistry, and mineral physics considerations. J. Geophys. Res., Solid Earth 108.

Niu, Y., Collerson, K.D., Batiza, R., Wendt, J.I., Regelous, M., 1999. Origin of enriched, E-type mid-ocean ridge basalt at ridges far from mantle plumes: The East Pacific Rise at 11°20′ N. J. Geophys. Res. 104, 7067–7087.

Ozawa, A., Tagami, T., Garcia, M.O., 2005. Unspiked K–Ar dating of the Honolulu rejuvenated and Ko'olau shield volcanism on O'ahu, Hawai'i. Earth Planet. Sci. Lett. 232, 1–11.

Parman, S.W., Grove, T.L., 2004. Harzburgite melting with and without H_2O: experimental data and predictive modeling. J. Geophys. Res. 109, B02201.

Pearce, J.A., Parkinson, I.J., 1993. Trace element models for mantle melting: application to volcanic arc petrogenesis. In: Magmatic Processes and Plate Tectonics. Geol. Soc. (Lond.) Spec. Publ. 76, 373–403.

Pertermann, M., Hirschmann, M.M., 2003. Partial melting experiments on a MORB-like pyroxenite between 2 and 3 GPa: constraints on the presence of pyroxenite in basalt source regions from solidus location and melting rate. J. Geophys. Res., Solid Earth 108.

Pietruszka, A.J., Garcia, M.O., 1999. A rapid fluctuation in the mantle source and melting history of Kilauea Volcano inferred from the geochemistry of its historical summit lavas. J. Petrol. 40, 1321–1342.

Pilet, S., Baker, M.B., Stolper, E.M., 2008. Metasomatized lithosphere and the origin of alkaline lavas. Science 320, 916–919.

Poitrasson, F., Halliday, A.N., Lee, D.C., Levasseur, S., Teutsch, N., 2004. Iron isotope differences between Earth, Moon, Mars and Vesta as possible records of contrasted accretion mechanisms. Earth Planet. Sci. Lett. 223, 253–266.

Polyakov, V.B., Mineev, S.D., 2000. The use of Mössbauer spectroscopy in stable isotope geochemistry. Geochim. Cosmochim. Acta 64, 849–865.
Polyakov, V.B., Clayton, R.N., Horita, J., Mineev, S.D., 2007. Equilibrium iron isotope fractionation factors of minerals: reevaluation from the data of nuclear inelastic resonant X-ray scattering and Mossbauer spectroscopy. Geochim. Cosmochim. Acta 71, 3833–3846.
Prinzhofer, A., Lewin, E., Allegre, C., 1989. Stochastic melting of the marble cake mantle: evidence from local study of the East Pacific Rise at 12°50′ N. Earth Planet. Sci. Lett. 92, 189–206.
Prytulak, J., Elliott, T., 2007. TiO_2 enrichment in ocean island basalts. Earth Planet. Sci. Lett. 263, 388–403.
Ren, Z.-Y., Shibata, T., Yoshikawa, M., Johnson, K.T., Takahashi, E., 2006. Isotope compositions of submarine Hana Ridge lavas, Haleakala volcano, Hawaii: implications for source compositions, melting process and the structure of the Hawaiian plume. J. Petrol. 47, 255–275.
Robinson, J., Wood, B., Blundy, J., 1998. The beginning of melting of fertile and depleted peridotite at 1.5 GPa. Earth Planet. Sci. Lett. 155, 97–111.
Rouxel, O., Dobbek, N., Ludden, J., Fouquet, Y., 2003. Iron isotope fractionation during oceanic crust alteration. Chem. Geol. 202, 155–182.
Salters, V.J., Stracke, A., 2004. Composition of the depleted mantle. Geochem. Geophys. Geosyst. 5.
Salters, V.J., Zindler, A., 1995. Extreme $^{176}Hf/^{177}Hf$ in the sub-oceanic mantle. Earth Planet. Sci. Lett. 129, 13–30.
Salters, V.J.M., Mallick, S., Hart, S.R., Langmuir, C.E., Stracke, A., 2011. Domains of depleted mantle: new evidence from hafnium and neodymium isotopes. Geochem. Geophys. Geosyst. 12.
Schoenberg, R., von Blanckenburg, F., 2006. Modes of planetary-scale Fe isotope fractionation. Earth Planet. Sci. Lett. 252, 342–359.
Schuessler, J.A., Schoenberg, R., Sigmarsson, O., 2009. Iron and lithium isotope systematics of the Hekla volcano, Iceland – evidence for Fe isotope fractionation during magma differentiation. Chem. Geol. 258, 78–91.
Sen, G., Frey, F.A., Shimizu, N., Leeman, W.P., 1993. Evolution of the lithosphere beneath Oahu, Hawaii – rare-earth element abundances in mantle xenoliths. Earth Planet. Sci. Lett. 119, 53–69.
Sen, G., Keshav, S., Bizimis, M., 2005. Hawaiian mantle xenoliths and magmas; composition and thermal character of the lithosphere. Am. Mineral. 90, 871–887.
Sen, I.S., Bizimis, M., Sen, G., 2010. Geochemistry of sulfides in Hawaiian garnet pyroxenite xenoliths: implications for highly siderophile elements in the oceanic mantle. Chem. Geol. 273, 180–192.
Sen, I.S., Bizimis, M., Sen, G., Huang, S., 2011. A radiogenic Os component in the oceanic lithosphere? Constraints from Hawaiian pyroxenite xenoliths. Geochim. Cosmochim. Acta 75, 4899–4916.
Sigmarsson, O., Carn, S., Carracedo, J.C., 1998. Systematics of U-series nuclides in primitive lavas from the 1730–36 eruption on Lanzarote, Canary Islands, and implications for the role of garnet pyroxenites during oceanic basalt formations. Earth Planet. Sci. Lett. 162, 137–151.
Sobolev, A.V., Hofmann, A.W., Sobolev, S.V., Nikogosian, I.K., 2005. An olivine-free mantle source of Hawaiian shield basalts. Nature 434, 590–597.
Sobolev, A.V., Hofmann, A.W., Kuzmin, D.V., Yaxley, G.M., Arndt, N.T., Chung, S.L., Danyushevsky, L.V., Elliott, T., Frey, F.A., Garcia, M.O., Gurenko, A.A., Kamenetsky, V.S., Kerr, A.C., Krivolutskaya, N.A., Matvienkov, V.V., Nikogosian, I.K., Rocholl, A., Sigurdsson, I.A., Sushchevskaya, N.M., Teklay, M., 2007. The amount of recycled crust in sources of mantle-derived melts. Science 316, 412–417.
Stracke, A., Salters, V.J.M., Sims, K.W.W., 1999. Assessing the presence of pyroxenite in the source of Hawaiian basalts: hafnium–neodymium–thorium isotope evidence. Geochem. Geophys. Geosyst. 1999GC000013.
Stracke, A., Hofmann, A.W., Hart, S.R., 2005. FOZO, HIMU, and the rest of the mantle zoo. Geochem. Geophys. Geosyst. 6.
Stracke, A., Snow, J.E., Hellebrand, E., von der Handt, A., Bourdon, B., Birbaum, K., Guenther, D., 2011. Abyssal peridotite Hf isotopes identify extreme mantle depletion. Earth Planet. Sci. Lett. 308, 359–368.
Teng, F.Z., Dauphas, N., Helz, R.T., 2008. Iron isotope fractionation during magmatic differentiation in Kilauea Iki Lava Lake. Science 320, 1620–1622.
Teng, F.Z., Dauphas, N., Huang, S., Marty, B., 2013. Iron isotopic systematics of oceanic basalts. Geochim. Cosmochim. Acta 107, 12–26.
Vlastelic, I., Aslanian, D., Dosso, L., Bougault, H., Olivet, J., Geli, L., 1999. Large-scale chemical and thermal division of the Pacific mantle. Nature 399, 345–350.
Vlastelic, I., Lewin, E., Staudacher, T., 2006. Th/U and other geochemical evidence for the Reunion plume sampling a less differentiated mantle domain. Earth Planet. Sci. Lett. 248, 379–393.
Weyer, S., Ionov, D.A., 2007. Partial melting and melt percolation in the mantle: the message from Fe isotopes. Earth Planet. Sci. Lett. 259, 119–133.
Weyer, S., Anbar, A.D., Brey, G.P., Munker, C., Mezger, K., Woodland, A.B., 2005. Iron isotope fractionation during planetary differentiation. Earth Planet. Sci. Lett. 240, 251–264.
White, W.M., Hofmann, A.W., 1982. Mantle heterogeneity and isotopes in oceanic basalts. Nature 295, 363–364.
Williams, H.M., McCammon, C.A., Peslier, A.H., Halliday, A.N., Teutsch, N., Levasseur, S., Burg, J.P., 2004. Iron isotope fractionation and the oxygen fugacity of the mantle. Science 304, 1656–1659.
Williams, H.M., Peslier, A.H., McCammon, C., Halliday, A.N., Levasseur, S., Teutsch, N., Burg, J.P., 2005. Systematic iron isotope variations in mantle rocks and minerals: the effects of partial melting and oxygen fugacity. Earth Planet. Sci. Lett. 235, 435–452.
Williams, H.M., Nielsen, S.G., Renac, C., Griffin, W.L., O'Reilly, S.Y., McCammon, C.A., Pearson, N., Viljoen, F., Alt, J.C., Halliday, A.N., 2009. Fractionation of oxygen and iron isotopes by partial melting processes: implications for the interpretation of stable isotope signatures in mafic rocks. Earth Planet. Sci. Lett. 283, 156–166.
Williams, H.M., Wood, B.J., Wade, J., Frost, D., Tuff, J., 2012. Isotopic evidence for internal oxidation of the Earth's mantle. Earth Planet. Sci. Lett., 321–322.
Wirth, R., Rocholl, A., 2003. Nanocrystalline diamond from the Earth's mantle underneath Hawaii. Earth Planet. Sci. Lett. 211, 357–369.
Woodland, A., Koch, M., 2003. Variation in oxygen fugacity with depth in the upper mantle beneath the Kaapvaal craton, Southern Africa. Earth Planet. Sci. Lett. 214, 295–310.
Workman, R.K., Hart, S.R., Jackson, M., Regelous, M., Farley, K.A., Blusztajn, J., Kurz, M., Staudigel, H., 2004. Recycled metasomatized lithosphere as the origin of the enriched mantle II (EM2) end-member: evidence from the Samoan volcanic chain. Geochem. Geophys. Geosyst. 5.
Zindler, A., Hart, S., Frey, F., Jakobsson, S., 1979. Nd and Sr isotope ratios and rare earth element abundances in Reykjanes Peninsula basalts evidence for mantle heterogeneity beneath, Iceland. Earth Planet. Sci. Lett. 45, 249–262.
Zindler, A., Staudigel, H., Batiza, R., 1984. Isotope and trace element geochemistry of young Pacific seamounts: implications for the scale of upper mantle heterogeneity. Earth Planet. Sci. Lett. 70, 175–195.